Automated Microaneurysm Segmentation and Detection using Generalized Eigenvectors

P M D S Pallawala[1] Wynne Hsu[1] Mong Li Lee[1] Say Song Goh[2]

[1]School of Computing,
National University of Singapore,
Singapore
email: {pererapa, whsu, leeml}
@comp.nus.edu.sg

[2]Department of Mathematics,
National University of Singapore,
Singapore

email: matgohss@nus.edu.sg

Abstract

Diabetic retinopathy is a major cause of blindness and microaneurysms are the first clinically observable manifestations of diabetic retinopathy. Regular screening and timely intervention can halt or reverse the progression of this disease. This paper describes an approach that is based on the generalized eigenvectors of affinity matrix to extract microaneurysms from digital retinal images. Microaneurysms are in the low intensity regions and detection is complicated by their small sizes, the presence of retinal vessels, and their similarity to another type of retinal abnormality – haemorrhages. In order to accurately detect microaneurysms, the affinity matrix is defined to suppress larger structures such as blood vessels, haemorrhages, etc and to create uniform affinity distribution for pixels belonging to microaneurysms. The generalized eigenvector solution seeks to find the optimal segmentation for microaneurysms and provides indication to the possible locations of microaneurysms. We differentiate the true microaneurysms by studying their feature characteristics. Experiments on 70 retinal sub-images of diabetic patients indicate that we are able to achieve 93% accuracy in the detection of microaneurysms.

1 Introduction

Diabetic retinopathy is a serious complication of diabetes mellitus and a major cause of blindness worldwide [4]. Microaneurysms are the first clinically observable lesions indicating diabetic retinopathy. A positive correlation has been demonstrated between the number of microaneurysms and the severity and progression of retinopathy [5]. Early detection and timely treatment of diabetic retinopathy can halt or reverse the progression of this disease and prevent blindness. For this reason, diabetic patients are encouraged to go for a yearly screening of their retina. A digital fundus camera is typically used to capture images of the retina. These images are subsequently read and graded by ophthalmologists. To reduce the workload of ophthalmologists and improve the follow-up management of diabetic patients, an automated detection of retinal abnormalities is essential.

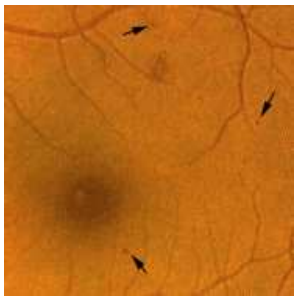

Figure 1: Section of a digital retinal image showing multiple microaneurysms (indicated by the black arrows).

Microaneurysms are dark reddish in color (Figure 1), and range from 25 – 100 microns in size. Microaneurysms occurring in the macula can lead to significant visual impairment. Existing algorithms to detect microaneurysms [2], [3], [7], [8], [13] and [14] are neither sufficiently sensitive, nor specific enough for clinical application. The main obstacle is the extreme variability in the color of the retinal images due to factors such as the degree of pigmentation in the retinal pigment epithelium, choroid in the eye, size of the pupil, and illumination. These factors in turn affect the appearance of microaneurysms in the retinal images.

Figure 2 shows the wide variation of microaneurysms color and background color in retinal images. In addition, the presence of haemorrhages (Figure 3(a)), retinal vessels (Figure 3(b)) and other diabetic retinopathy related abnormalities, such as hard exudates (Figure 3(c)) further complicate the detection of microaneurysms.

In this work, we devise a generalized eigenvector based

method to extract microaneurysms from retinal images. We will demonstrate how a generalized eigenvector solution is able to provide an indicator to the location of microaneurysms. These locations are analyzed using microaneurysm specific features to identify the true microaneurysms. Experiments on 70 retinal sub-images of diabetic patients indicate that we are able to achieve 93% accuracy in the detection of microaneurysms.

Figure 2: Wide variation in the color of microaneurysms and background color.

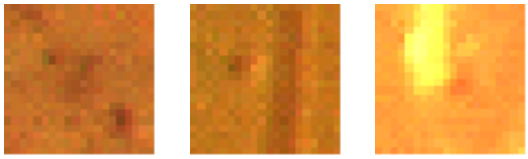

(a) (b) (c)

Figure 3: Microaneurysms occurring near (a) hemorrhage (dark reddish areas), (b) vessels (dark reddish line) and (c) hard exudates (bright yellowish area).

2 Related Work

Majority of microaneurysm detection research has been focused on the detection of microaneurysms from fluorescein angiography [2], [7] and [14]. During fluorescein angiography, microaneurysms become hyper-fluorescent and edges are well defined compared to digital retinal images. This makes the detection of microaneurysms from fluorescein angiograms less complex compared to that from fundus camera images.

Kamel et. al. [7] implemented a learning vector quantization neural network to detect microaneurysms from fluorescein angiograms based on multi-stage training procedure. While this approach effectively improved the accuracy rate, it required longer training periods to achieve the desired accuracy. Spencer et. al. [14] applied binary morphological and thresholding techniques to detect microaneurysms from fluorescein angiograms. These techniques suffer due to the presence of retinal vessels and background color variations. To improve specificity, Spencer et. al. [13] used a region growing algorithm to identify the candidate's morphology, and a feature classification algorithm to distinguish the microaneurysms. While this is a significant improvement, the region growing algorithm remains sub-optimal. Cree et. al. [2] implemented an improved area growing and feature based classification tool, and achieved 82% accuracy in the detection of microaneurysms.

Ege et. al. [3] described a tool for the automatic analysis of digital retinal images, and evaluated classifiers such as Bayes classifier, Mahalanobis classifier and KNN on an array of features such as log(area), minor axis variance, major axis variance, etc. Among them, the Bayes classifier and KNN classifier showed promising results, but their approach requires a pre-processing step that involves mean filtering and thresholding. Small microaneurysms are removed during the filtering step, while thresholding is not effective given the variations in background intensity.

3 Eigenvector Based Segmentation Methods

Various eigenvector based segmentation methods have been developed in [1], [9], [10], [11], [12] and [15] for the automatic grouping and segmentation problems in computer vision applications. Image segmentation methods using eigenvectors are based on eigenvectors of affinity matrix. An affinity matrix represents the feature similarity between a given point in an image with all the points in the image. The calculation of feature similarity is based on the Euclidean distance, intensity and etc. The simplest form of an affinity matrix W with entries $W(i,j)$ is defined by

$$W(i,j) = e^{-\frac{d(X(i),X(j))^2}{d_0^2}}, \quad (1)$$

where d_0 is a reference distance below which two points are considered to be similar and beyond which two points are treated as dissimilar; and $d(X(i),X(j))$ is defined as $\|X(i) - X(j)\|$, the Euclidean distance between the points $X(i)$ and $X(j)$.

Note that different definitions of affinity matrix are possible. The affinities do not have to obey the metric axioms (e.g. [6]) and only assume that $d(X(i),X(j)) = d(X(j),X(i))$. We now review two algorithms that are based on eigenvectors of affinity matrices and examine their feasibility to microaneurysm detection.

3.1 Perona and Freeman's Algorithm

Perona and Freeman [9] proposed an eigenvector based technique to discover the foreground group in a scene based on affinity matrix. Experiments have shown good grouping performance of affinity factorization even on data sets where the background was unstructured.

The clustering algorithm in [9] is based on thresholding the first eigenvector of the affinity matrix defined by (1). Figure 4(b) shows the first eigenvector of the affinity matrix for sub-images in Figure 4(a). The eigenvectors shown here are normalized to help the visualization of the matrices. Indeed, the eigenvector separates microaneurysm in

the first sub-image from the background and clustering can be applied to identify the microaneurysms in this instance. However, we observe from the second and third sub-images that various noises arising from retinal vessels tend to complicate the segmentation process. Further examination of sub-images that contain exudates and haemorrhages show the inclusion of significant noise.

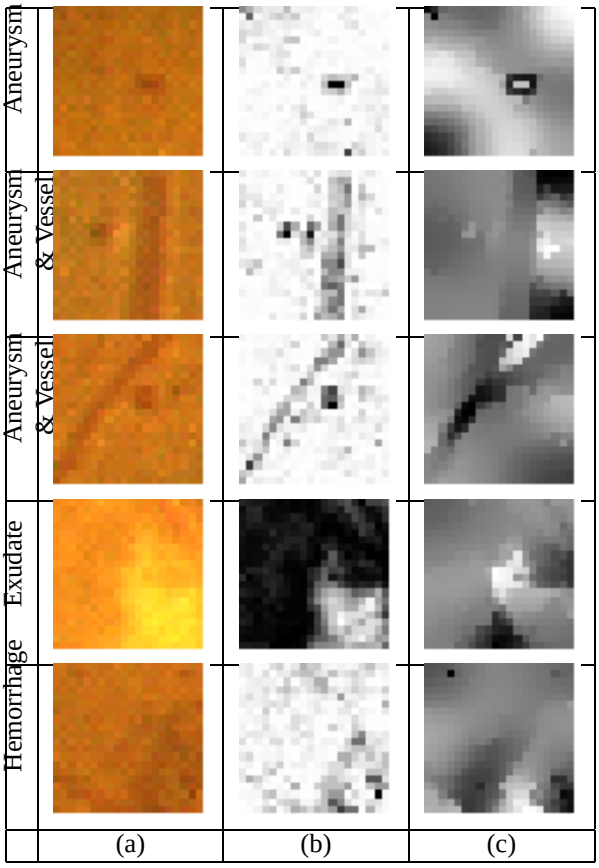

Figure 4: (a) 20×20 pixels sub-image, (b) Perona and Freeman's algorithm and (c) Shi and Malik's algorithm (parameter settings: $\rho_I = 60$, $\rho_X = 3$, $r = 3$).

3.2 Shi and Malik's Algorithm

Shi and Malik [12] proposed a novel approach to image segmentation by using a global criterion called normalized cut. The normalized cut algorithm was iteratively applied to the second smallest generalized eigenvector to achieve the segmentation. Experimental results showed that the normalized cut criterion was able to partition the spatial point sets into groups, but performed rather poorly in images with ill-defined boundaries.

In [12], to solve the segmentation problem, rather than examining the first eigenvector of W, generalized eigenvectors are used. A graph $G = (V, E)$ is created by treating each pixel as a node. The weight $W(i, j)$ of the edge between nodes i and j is defined as the product of a feature similarity term and spatial proximity term:

$$W(i,j) = e^{-\frac{\|I(i)-I(j)\|^2}{\rho_I^2}} f(i,j), \tag{2}$$

where

$$f(i,j) = \begin{cases} e^{-\frac{\|X(i)-X(j)\|^2}{\rho_X^2}}, & \text{if } \|X(i)-X(j)\| < r, \\ 0, & \text{otherwise,} \end{cases} \tag{3}$$

$I(i)$ and $X(i)$ are the intensity value and spatial location of node i respectively, and ρ_I, ρ_X and r are positive constants.

To review the concept of normalized cut, let the graph $G = (V, E)$ be partitioned into two disjoint sets A and B, i.e. $A \cup B = V$, $A \cap B = \emptyset$. Then the normalized cut is defined as

$$\text{Ncut}(A,B) = \frac{\text{cut}(A,B)}{\text{assoc}(A,V)} + \frac{\text{cut}(A,B)}{\text{assoc}(B,V)}, \tag{4}$$

where

$$\text{cut}(A,B) = \sum_{i \in A,\, j \in B} W(i,j) \tag{5}$$

and

$$\text{assoc}(A,V) = \sum_{i \in A,\, j \in V} W(i,j). \tag{6}$$

The normalized cut measures the affinity between groups normalized by the affinity within each group. Let D be the diagonal matrix with diagonal entries given by $D(i,i) = \sum_{j \in V} W(i,j)$, where $i \in V$. As shown in [12], by considering the real value domain, an approximate solution to the discrete problem of finding segmentation that minimizes the normalized cut is given by the second smallest generalized eigenvector y of the equation

$$(D - W)y = \lambda D y. \tag{7}$$

Figure 4(c) shows the second smallest generalized eigenvector of (7) for the sub-images. Although in the first two cases, this vector can be segmented to detect the microaneurysm, the last three cases do not provide the required segmentation.

4 Generalized Eigenvector Based Microaneurysm Detection

In this work, we devise a generalized eigenvector based method to extract microaneurysms from retinal images by suppressing vessels and other structures. There are two steps in the proposed microaneurysm detection algorithm:

1. Extract microaneurysm points using generalized eigenvectors.
2. Utilize microaneurysm specific features to identify the true microaneurysms.

We will explain each step in the following subsections.

4.1 Extract Microaneurysm Points

We define the affinity function using the feature similarity term and spatial proximity term according to (2). However as the microaneurysms are in the low intensity region, in contrast to (3), we define the spatial proximity term $f(i,j)$ as

$$f(i,j) = \begin{cases} 0, & \text{if } \|X(i) - X(j)\| < r, \\ e^{-\frac{\|X(i)-X(j)\|^2}{\rho_X^2}}, & \text{otherwise.} \end{cases}$$

This allows us to create a uniform affinity for microaneurysm pixels as this step sets affinity of any given two microaneurysm pixels to zero. As the dimensions of vessels, and haemorrhages are larger than the selected r value for microaneurysms, their affinities are brought close to the background affinities. The intention of this definition is to create uniform low affinity level for microaneurysms and uniform high affinity level for the background and other structures such as vessels.

A retinal image can be bipartitioned to background region (background and other structures such as vessels, haemorrhages, etc.) and micro-region (microaneurysm region) by minimizing association of background region and maximizing dissociation of micro-region. Let the background region and micro-region be A and B respectively. Minimizing the association of region A prevents tightly grouped background region and allows closely related other affinity groups to be segmented with the background region. By maximizing dissociation of region B, it facilitates segmentation of tightly grouped small objects such as microaneurysms. Therefore the desired segmentation can be achieved by minimizing the cost function

$$\text{segment}(A,B) = \frac{\text{assoc}(A,A)}{\text{assoc}(A,V)} - \frac{\text{cut}(B,A)}{\text{assoc}(B,V)}.$$

Using (5), (6) and (4), we have

$$\begin{aligned} \text{segment}(A,B) &= \frac{\text{assoc}(A,V) - \text{cut}(A,B)}{\text{assoc}(A,V)} \\ &\quad - \frac{\text{cut}(B,A)}{\text{assoc}(B,V)} \\ &= 1 - \frac{\text{cut}(A,B)}{\text{assoc}(A,V)} - \frac{\text{cut}(B,A)}{\text{assoc}(B,V)} \\ &= 1 - \text{Ncut}(A,B). \end{aligned} \tag{8}$$

Let $x = (x_1, \ldots, x_N)^T$, where $N = |V|$, be an indicator vector such that $x_i = 1$ if node i is in A and -1, otherwise. Then denoting $\text{Ncut}(A,B)$ as $\text{Ncut}_W(x)$ with the $N \times N$ affinity matrix W, the derivation in [12] shows that

$$\begin{aligned} \text{Ncut}_W(x) &= \frac{\sum_{x_i>0,\, x_j<0} -w_{ij}x_ix_j}{\sum_{x_i>0} d_i} \\ &\quad + \frac{\sum_{x_i<0,\, x_j>0} -w_{ij}x_ix_j}{\sum_{x_i<0} d_i}, \end{aligned} \tag{9}$$

where $w_{ij} = W(i,j)$ and $d_i = \sum_{j=1}^N w_{ij}$. Further, writing $\text{segment}(A,B)$ as $\text{segment}(x)$, it follows from (8) that

$$\min_x \text{segment}(x) = 1 - \max_x \text{Ncut}_W(x). \tag{10}$$

To solve this extremal problem, first let D be the diagonal matrix $\text{diag}(d_i)_{i=1}^N$. Our strategy is to find an $N \times N$ symmetric matrix $\widetilde{W}$ such that $\max_x \text{Ncut}_W(x) = -\min_x \text{Ncut}_{\widetilde{W}}(x)$. Indeed, defining

$$\widetilde{W} = 2D - W, \tag{11}$$

since D is diagonal and W is symmetric, $\widetilde{W}$ is also symmetric. Writing $\widetilde{W} = (\widetilde{w}_{ij})_{i,j=1}^N$, we have

$$\widetilde{w}_{ij} = \begin{cases} -w_{ij}, & \text{if } i \neq j, \\ 2d_i - w_{ii}, & \text{if } i = j. \end{cases} \tag{12}$$

Let $\widetilde{D}$ be the diagonal matrix $\text{diag}(\widetilde{d}_i)_{i=1}^N$, where $\widetilde{d}_i = \sum_{j=1}^N \widetilde{w}_{ij}$. Then (12) implies that

$$\widetilde{d}_i = 2d_i - \sum_{j=1}^N w_{ij} = 2d_i - d_i = d_i, \tag{13}$$

and so $\widetilde{D} = D$.

Based on $\widetilde{W}$ and $\widetilde{D}$, and using the definition in (9), it follows from (12) and (13) that $\text{Ncut}_{\widetilde{W}}(x) = -\text{Ncut}_W(x)$ and hence

$$\max_x \text{Ncut}_W(x) = -\min_x \text{Ncut}_{\widetilde{W}}(x). \tag{14}$$

In other words, the problem of maximizing the normalized cut with respect to an affinity matrix W is equivalent to that of minimizing the normalized cut with respect to the new affinity matrix $\widetilde{W}$ given by (11). Results on the minimization of normalized cut are available in [12], which show that

$$\min_x \text{Ncut}_{\widetilde{W}}(x) = \min_y \frac{y^T(\widetilde{D} - \widetilde{W})y}{y^T\widetilde{D}y}, \tag{15}$$

with the minimization on the right-hand side taken over all $y = (y_1, \ldots, y_N)^T$ satisfying $y_i \in \{1, -b\}$ and $y^T\widetilde{D}1_N = 0$, where $b = \left(\sum_{x_i>0} \widetilde{d}_i\right) \Big/ \left(\sum_{x_i<0} \widetilde{d}_i\right)$ and 1_N is an $N \times 1$ vector of all ones.

As shown in [12], if y is relaxed to take real values, an approximate solution to the minimization problem (15) is given by the second smallest eigenvector of the generalized eigenvalue system

$$(\widetilde{D} - \widetilde{W})y = \widetilde{\lambda}\widetilde{D}y. \tag{16}$$

Using (11) and (13), (16) is equivalent to the generalized eigenvalue system

$$Wy = \lambda Dy, \tag{17}$$

where $\lambda = \widetilde{\lambda} + 1$. Note that y is the second smallest eigenvector of (16) if and only if it is the second smallest eigenvector of (17). Consequently, it follows from (14) and (15) that an approximate solution of the minimization problem (10) is given by the second smallest eigenvector of (17). Figure 5 shows the second smallest eigenvector obtained and it clearly indicates the position of microaneurysm in the image, in contrast to the results in figure 4. Further, the algorithm is not affected by the presence of blood vessels, haemorrhages and etc.

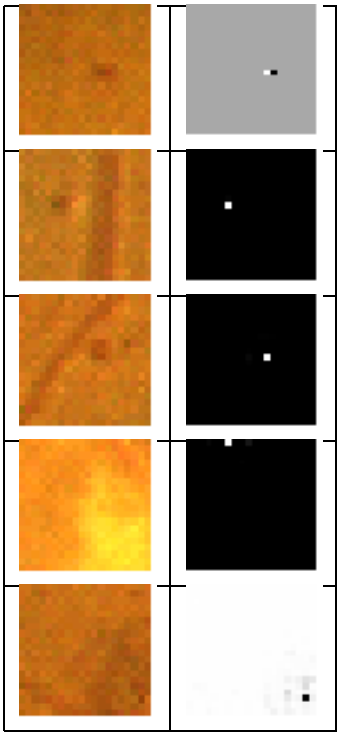

Figure 5: (a) Sub-images and (b) second smallest eigenvector (parameter settings: $\rho_I = 60, \rho_X = 3, r = 3$).

4.2 Identify True Microaneurysms

The probable locations of the microaneurysms are determined by the position (u_m,v_m) of the highest absolute value of the second smallest eigenvector. Using this position, we define $I_{\text{difference}}$ as

$$I_{\text{difference}} = I_c - I_{bc},$$

where I_c is the intensity value of the (u_m,v_m) coordinates and I_{bc} is the mean intensity value of all the pixels belonging to the immediate background (4×4 pixels area centered on (u_m,v_m)). The computation of $I_{\text{difference}}$ was initially carried out with a training set containing 11 sub-images (including microaneurysms and others). Figure 6 shows the distribution of $I_{\text{difference}}$ for the microaneurysms and, other abnormalities and structures e.g. hemorrhages, retinal vessels and hard exudates. The distribution reveals that the microaneurysms are linearly separable at this stage. Indeed, true microaneurysms can be detected by setting the threshold value of $I_{\text{difference}}$ to be 7, above which indicate microaneurysms and below which other abnormalities and structures. Figure 7 shows the results obtained by using the feature $I_{\text{difference}}$ on generalized eigenvectors.

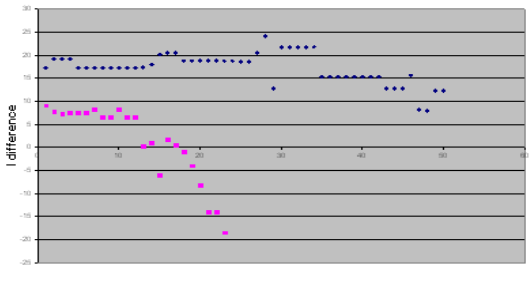

Figure 6: $I_{\text{difference}}$ distribution (x-axis: abnormality index, diamond: microaneurysms and square: others).

5 Experiment Results

Our image database consists of digital retinal images derived from diabetic retinopathy screening program and contain the standard 40 degree field of retina centered on macula. Image resolution is 25 microns/pixel, and therefore microaneurysm diameter is between 3-4 pixels. We evaluate the robustness and reliability of our segmentation and detection algorithm on 70 sub-images containing microaneurysms. These sub-images contain structures such as retinal vessels and abnormalities such as hemorrhages, exudates and etc. A retinal specialist first reviewed these images and identified the locations and types of lesions present in the images. We compare the results of our algorithm with that given by the retinal specialist.

	Number of Sub-Images
Correctly classified cases	65
Incorrectly classified cases	5

Table 1: Results of microaneurysm detection algorithm.

The algorithm correctly classified microaneurysms in 65 cases and failed in 5 cases (Table 1). The incorrectly classified cases (Figure 8) occurred in cases where the microaneurysm is blurred and other structures were detected in these cases as microaneurysms. Experiments on 70 microaneurysms sub-images of diabetic patients indicate that we are able to achieve 93% accuracy in the detection of microaneurysms.

6 Conclusion

In this work, we have proposed a microaneurysm segmentation and detection algorithm that is based on generalized eigenvectors of affinity matrix. The proposed technique is

robust and has a minimal interference from other structures and lesions. Experiments on digital retinal images indicate that we are able to achieve 93% accuracy in the detection of microaneurysms.

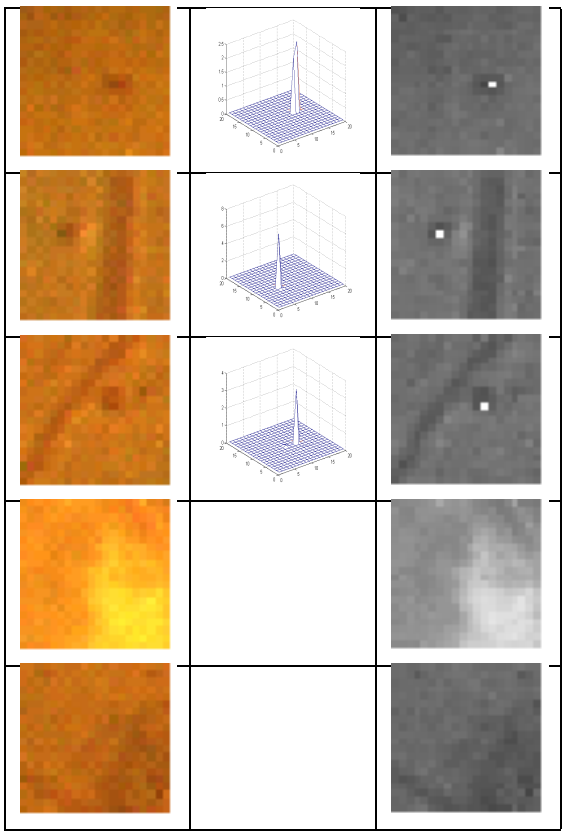

Figure 7: (a) Sub-images, (b) second smallest eigenvector for the microaneurysm and (c) microaneurysm location highlighted in the green layer (only the first three sub-images contain microaneurysms).

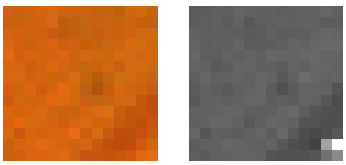

Figure 8: Sample of incorrectly classified case.

References

[1] J. Costeira and T. Kanade, A Multibody Factorization Method for Independently Moving Objects, *International Journal of Computer Vision*, Vol. 29(3), pp. 159-179, 1998.

[2] M.J. Cree, J.A. Olson, K.C. McHardy, J.V. Forrester, P.F. Sharp, Automated Microaneurysm Detection, *Proceedings of International Conference on Image Processing*, Vol. 3, pp. 699-702, 1996.

[3] B.M. Ege, O.K. Hejlesen, O.V. Larsen, K. Møller, B. Jennings, D. Kerr, D.A. Cavan, Screening for Diabetic Retinopathy Using Computer Based Image Analysis and Statistical Classification, *Computer Methods and Programs in Biomedicine*, Vol. 62, pp. 165-175, 2000.

[4] A.M.P. Hamilton, M.W. Ulbig, P. Polkinghorne, *Management of Diabetic Retinopathy*, BMJ Publishing Group, 1996.

[5] T. Hellstedt and I. Immonen, Disappearance and Formation Rates of Microaneurysms in Early Diabetic Retinopathy, *British Journal of Ophthalmology*, Vol. 80, pp. 135-139, 1996.

[6] D.W. Jacobs, D. Weinshall, Y. Gdalyahu, Classification with Nonmetric Distances: Image Retrieval and Class Representation, *IEEE Transactions on Pattern Analysis and Machine Intelligence*, Vol. 22(6), pp. 583-600, 2000.

[7] M. Kamel, S. Belkassim, A.M. Mendonca, A. Campilho, A Neural Network Approach for the Automatic Detection of Microaneurysms in Retinal Angiograms, *Proceedings of International Joint Conference on Neural Networks*, Vol. 4, pp. 2695-2699, 2001.

[8] A.M. Mendonca, A.J. Campilho, J.M. Nunes, Automatic Segmentation of Microaneurysms in Retinal Angiograms of Diabetic Patients, *Proceedings of International Conference on Image Processing*, pp. 728-733, 1999.

[9] P. Perona and W. Freeman, A Factorization Approach to Grouping, *Proceedings of European Conference on Computer Vision*, Vol. 1, pp. 655-670, 1998.

[10] S. Sarkar and K.L. Boyer, Quantitative Measures of Change Based on Feature Organization: Eigenvalues and Eigenvectors, *Proceedings of IEEE Conference on Computer Vision and Pattern Recognition*, pp. 478-483, 1996.

[11] G.L. Scott and H.C. Longuet-Higgins, Feature Grouping by Relocation of Eigenvectors of the Proximity Matrix, *Proceedings of British Machine Vision Conference*, pp. 103-108, 1990.

[12] J. Shi and J. Malik, Normalized Cuts and Image Segmentation, *IEEE Transactions on Pattern Analysis and Machine Intelligence*, Vol. 22(8), pp. 888-905, 2000.

[13] T. Spencer, J.A. Olson, K.C. McHardy, P.F. Sharp, J.V. Forrester, An Image-Processing Strategy for the Segmentation and Quantification of Microaneurysms in Fluorescein Angiograms of the Ocular Fundus, *Computers and Biomedical Research*, Vol. 29, pp. 284-302, 1996.

[14] T. Spencer, R.P. Phillips, P.F. Sharp, J.V. Forrester, Automated Detection and Quantification of Microaneurysms in Fluorescein Angiograms, *Graefe's Archives of Clinical and Experimental Ophthalmology*, Vol. 230, pp. 36-41, 1992.

[15] Y. Weiss, Segmentation Using Eigenvectors: a Unifying View, *Proceedings of IEEE International Conference on Computer Vision*, pp. 975-982, 1999.